
Object detection for crabs in top-view seabed imagery

Vlad Velici

School of Electronics and Computer Science
University of Southampton
Southampton, UK

Adam Prügel-Bennett

School of Electronics and Computer Science
University of Southampton
Southampton, UK

Abstract

This report presents the application object detection on a database of underwater images of different species of crabs, as well as aerial images of sea lions and Pascal VOC. The model is an end-to-end object detection model based on a convolutional network and a Long Short-Term Memory detector.

1 Introduction

This report presents the problem of object detection and classification, popular datasets, and in Section 1.1 we present the datasets relevant to this work.

Image classification is the task of labelling an image with a class. Given an input image a model must predict what class it belongs to. Images used for classification often have one large central object. However this is not the case in real life where we are surrounded by many objects. A more challenging task is to predict where all the objects are in an image and what class they belong to. We call this object detection. An intermediary objective can be object localisation which is simply the task of finding all objects in an image but not assigning a class to them.

Depending on the actual dataset and desired end result, an object is defined by its class and either its x and y coordinates or a bounding box (x , y coordinates, width w and height h). We will use the term object coordinates to refer to either x and y coordinates or a bounding box.

Datasets like PASCAL Visual Object Classes (object detection challenge) (Everingham et al., 2015) and COCO (Lin et al., 2014) have bounding box coordinates, where other datasets like the ones used in the NOAA Fisheries Steller Sea Lion Population Count Kaggle competition (NOAA Fisheries, 2017) and the data obtained from (Thornton et al., 2016) only have the centre coordinate of the objects. Semantic segmentation is a type of object detection where the bounding boxes or coordinates are replaced with object boundaries at pixel level. We are not looking into semantic segmentation in this report at this time.

1.1 Crabs and Steller Sea Lions datasets

Steller Sea Lion population started to decline in the 1970s, and in 1990 it was listed as a threatened species. NOAA Fisheries divided the population into the western stock and the eastern stock, the separation line being at 144 deg West longitude. The eastern stock population started to recover in the late 1970s and has fully recovered in 2013. However, the western stock population has not. The population in the eastern side of the western stock (144 deg - 170 deg West longitude) is increasing, but the western end, in Aleutian Islands, continues to decline. A map of the locations can be seen in Figure 1. NOAA Fisheries is working on creating long-term population trends over time to help develop recovering strategies for the endangered population. Having such trends and tools will allow NOAA to make better decisions about managing fisheries and to identify possible threats affecting the endangered populations (Fritz et al., 2016).

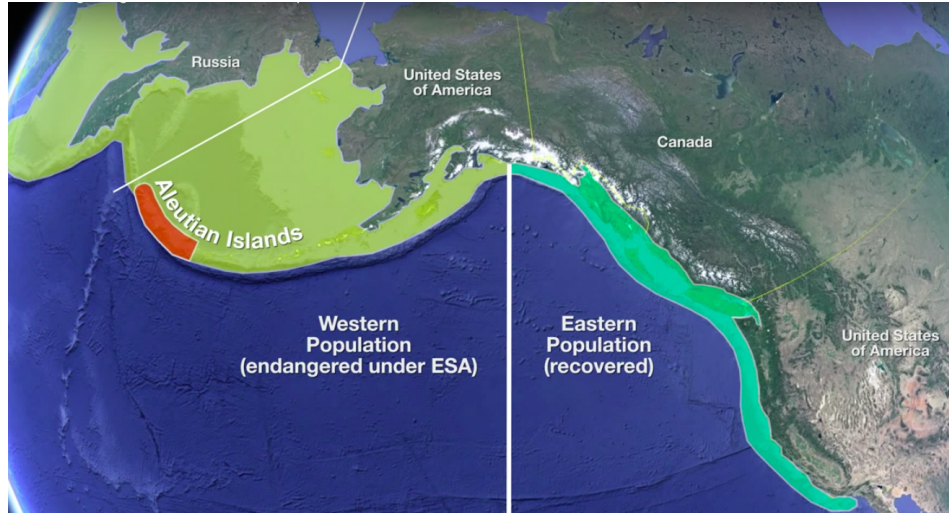


Figure 1: Map of Steller Sea Lion populations from NOAA Fisheries outreach video <https://youtu.be/oiL8tDCqzy4>. Red area shows the endangered population, yellow area shows the population that is increasing and green area shows the population that has fully recovered in 2013.

NOAA Fisheries can now gather large amounts of aerial imagery efficiently using drones. They are, however, facing the problem of manually labelling the images to be able to create population trends. Currently they use human labelling but this method is prone to errors and slow, thus they are seeking automated solutions to improve the speed and quality of labelling. They have launched a Kaggle¹ competition to invite data scientists to find solutions and implement models to solve the labelling problem. The competition has a dataset of 100+GB of labelled imagery (NOAA Fisheries, 2017).

The work presented in Thornton et al. (2016) is a practical method of using underwater robots to survey large areas of seafloor (multi-hectare areas). The images produced were then processed to build 3D reconstructions and mosaics which were manually labelled for 6 taxa of animals (crabs, mussels and shrimps). Labelling taxa by hand is a long, slow, expensive and error prone process, and it is the bottleneck of the whole process of creating population densities and distributions efficiently. They produced a dataset of two labelled mosaics of imagery taken at two locations: C0014G_2m_2014 is a 1060m deep drill site in the Iheya North field, and NBC_2m_2014 is a naturally active site located 500m away.

In this report we will present a model created for these two datasets and report its performance, training and possible improvements.

1.1.1 Note on the state of the art

This work was part of my PhD *initial* project, which was done in 2016, for the purpose of exploring deep learning and object detection, not necessarily to obtain good results. If the reader is interested in exploring the field of object detection and building competitive models we suggest to look up the current state of the art models and methods. We refrain from mentioning any works here because they will quickly become out of date.

2 Crab detector network

In this report we present a deep neural network built for end-to-end object detection. As an end-to-end model, it takes as an input an image and outputs object coordinates, classes and confidence scores. The model can be configured to use centre coordinates of the objects or bounding boxes.

¹Kaggle: <https://kaggle.com/>

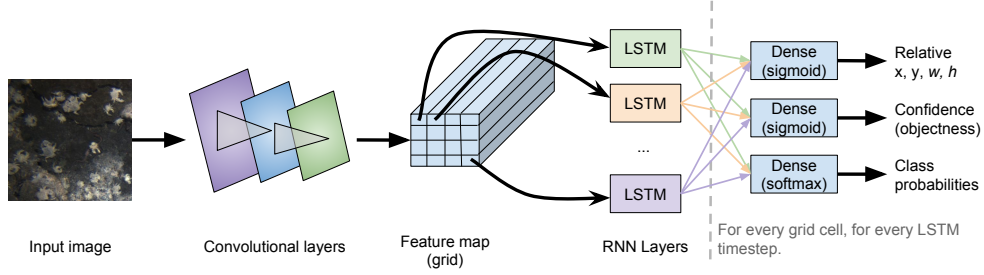


Figure 2: Architecture of our model.

The model is built for the crabs and sea lions datasets where objects are defined by centre coordinates and are relatively small but it is also evaluated on VOC12 where objects are described by bounding boxes.

3 Model architecture

The model architecture is based on Stewart et al. (2016). We improved on their model by adding a classifier and adapting the loss function. We also added support for x, y coordinates labels as well as bounding boxes to enable using the model on the Pascal VOC 2012 dataset, the crabs and the Steller Sea Lions datasets.

The model architecture is illustrated in Figure 2. For a forward pass, the model performs the following steps:

Step 1 The input image is fed into a Convolutional Neural Network (CNN). The feature map that results from the CNN is a $B \times W \times H \times F$ grid, where B is the batch size, W, H are the width and height of the grid and F is the number of filters in the last convolutional layer.

Step 2 Each of the $B \times W \times H$ grid cells (F -sized feature vectors) is fed into a layer of Long Short-Term Memory cells (LSTMs). Note that changes in W and H can be considered changes in the batch size B , therefore the model can be used for any input image size.

Step 3 At each recurrence the LSTM cells are densely connected to three different units: one to predict objectness (used as confidence score), one to predict class probabilities (softmax), and one to predict object coordinates relative to the centre of the grid cell.

For our experiments we use square input images of 224×224 pixels, therefore our grid is a square of size $G = W = H$. We use two CNN configurations that result in $G = 7$ and $G = 4$, respectively. Although we use a fixed image size as input, the model can support input images of any size as the LSTM and dense layers receive a fixed-size input regardless of the input image size. The grid size changes with the input image and affects how many times the LSTM and dense layers are run sequentially across the image.

A fixed number of recurrences (time steps) of the LSTM cells, k , is set. This is an implementation limitation. Theoretically, at test time the model can run recurrences until a stop symbol is produced (first object with confidence below a set threshold, e.g. 0.5). During training the model can have one recurrence for each ground truth label and an additional one for training the stop symbol. This can be used to speed up the computations.

There is no ground truth order in which the objects in an image must be predicted. Therefore simply matching predictions and ground truth labels as they appear would induce errors if the order does not match. For instance, if an image has objects A and B given in the ground truth labels in this order and the model predicts B, A, a direct matching would consider this prediction wrong, but in reality it is correct. As suggested by Stewart et al. (2016), the Hungarian method is used as an efficient way to match ground truth labels to predictions using the distance between the coordinates as the matching cost.

A new loss function was derived based on Stewart et al. (2016) and Redmon et al. (2016). The loss function l is the sum of three components: the confidence (objectness) loss l_o , the coordinates (regression) loss l_r and the class loss l_c .

For the following equations we consider the ground truth labels to be sorted such that the i^{th} element of predictions is matched to the i^{th} element of ground truth labels by the Hungarian method as described above.

The confidence score prediction is designed as a binary classification problem and we use softmax and cross-entropy loss for l_o .

The regression loss is a root mean squared error function that only penalises predictions where there is a real object. Define \mathbf{g}_o to be the vector of ground truth confidence scores with elements $g_o(1), \dots, g_o(n) \in \{0, 1\}$ where $n = G^2 * k$ is the number of predictions per image and $g_o(i) = 1$ if the prediction i is an object, 0 otherwise. Let $m = \sum_{i=1}^n g_o(i)$ be the number of real objects in the image, F_r to be a $n \times r$ matrix, where r is the number of coordinates required per object ($r = 2$ for x, y coordinates and $r = 4$ for bounding boxes) with elements $F_r(i, j)$ representing predicted coordinates. Similarly, let G_r be a matrix of the same size with elements containing ground truth coordinates or zeros if there is no object. We now define the regression loss

$$l_r = \sqrt{\frac{1}{m * r} \sum_{i=1}^n g_o(i) \sum_{j=1}^r (F_r(i, j) - G_r(i, j))^2}. \quad (1)$$

Let F_c be a $n \times C$ matrix (C is the number of classes) with rows $\mathbf{F}_c(\mathbf{i})$ representing the probabilities of each class for object i (output of softmax). Similarly let G_c be a similar matrix representing the ground truth. The class loss is

$$l_c = \frac{1}{m} \sum_{i=1}^n g_o(i) H(\mathbf{F}_c(\mathbf{i}), \mathbf{G}_c(\mathbf{i})), \quad (2)$$

where $H(\mathbf{a}, \mathbf{b})$ is the cross-entropy between \mathbf{a} and \mathbf{b} . Note this is the cross-entropy loss but it only penalises predictions where there is a real object (otherwise ground truth data does not exist for the class).

4 Preprocessing

The labels are pre-processed such that, for an image, we will have $G \times G \times k$ object labels in total, k for each grid cell. If there are more than k objects in a particular grid cell, we cap them at k and drop the rest. Less than 10 objects are dropped in the whole crabs dataset for $k = 8$. Objects with confidence 0 are appended if there are fewer than k labels.

Label coordinates are made relative to the centre of the grid cell. We say the top left corner of a grid cell is the point (0, 0) and the bottom right corner is the point (1, 1). The centre of the grid cell is at (0.5, 0.5). This forces the LSTMs to predict objects that belong to their grid cell and makes the network easier to train. In the case of bounding boxes, the width and height are relative to the input image size, such that an object with width and height 1 covers the whole input image. This allows the network to predict objects that are larger than a grid cell.

The image pixel values are normalised to fall between -0.5 and 0.5.

4.1 Crabs dataset

The crab dataset from Thornton et al. (2016) is made of two big mosaics C0014G_2m_2014 (20320×28448 pixels) and NBC_2m_2014 (20320×20320 pixels), each representing an imaging location. We slice the mosaics into 224×224 pixels images and randomly split them into training, cross-validation (dev) and test sets (60% – 20% – 20%).

The labels consist of manually labelled x and y coordinates of each individual and its species.

The dataset is heavily unbalanced, as seen in Table 1. This leads to hard to train models thus we split the dataset into two sub-datasets. We call **crabs** the dataset containing all images and **crabs-top3** the dataset consisting of the top 3 species by population count.

Table 1: Crabs species counts in the two locations (mosaics) and overall. The last column shows which species are in the **crabs-top3** dataset.

Species	C0014	NBC	Total	crabs-top3
Alvinocaridid	170	500	670	
Bathymodiolus japonicus	6,780	7,339	14,119	✓
Bathymodiolus platifrons	7,282	12,969	20,251	✓
Paralomis	96	109	205	
Shinkaia crosnieri	3,536	7,160	10,696	✓
Thermosipho desbruyesi	12	6	18	
Total individuals	17,876	28,083	45,959	45,066

Table 2: Sea Lions dataset population counts, showing the differences between the given population counts and the generated dots. The dots have 16,955 dots that could not reliably be classified by colour (not shown).

	Label counts	Dot counts	Δ
adult_males	5,392	5,349	43
subadult_males	4,345	4,028	317
adult_females	37,537	59,080	21,543
juveniles	20,118	20,895	777
pups	16,285	16,141	144
Totals	83,677	105,493	21,816

The big mosaics provided suffer from image quality loss as they are composed of individual higher-quality images, overlapped and transformed to form a map-like mosaic. The effect can be observed in Figure 3. The original images are available but, unfortunately, there is no mapping between the labels on the mosaic and the original images, which are unlabelled.

Sequentially slicing the mosaics results in a total of 2608 224×224 images. A dataset of such a small size is likely to make models easily overfit and hard to generalise. To address this issue we heavily augment the training set with random rotations, zooms, shears, and shifts and also use a different slicing technique where we cut an image centred on a crab. This results in a total of 45959 images (17,876 from C0014G and 28,083 from NBC) that have plenty of overlapping content.

4.2 Sea Lions dataset

The Steller Sea Lions dataset from the NOAA Kaggle competition (NOAA Fisheries, 2017) has many large aerial images. 948 for training and 18,636 for testing during the competition. Similarly to the crabs dataset, the dataset has x, y and class coordinates as labels, manually labeled.

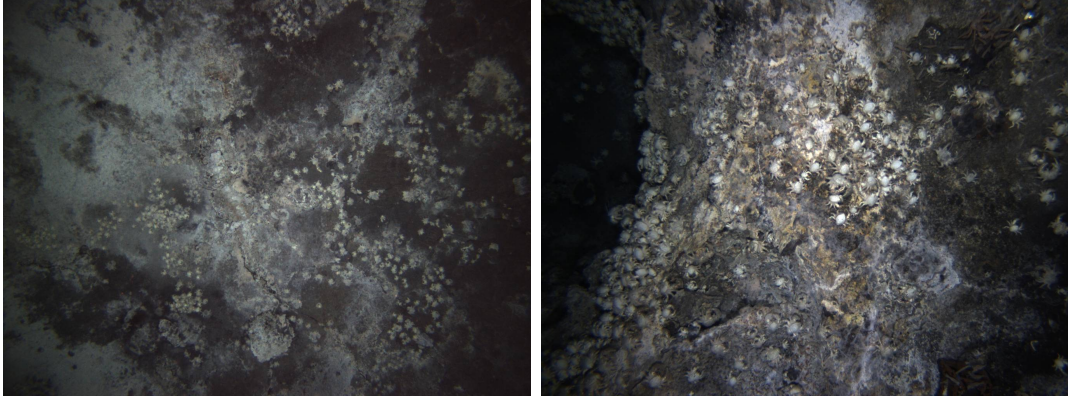
The labels are given in two ways. Population counts per image are given in a CSV file. The x, y coordinates are given in a second pair of training images annotated with coloured dots, the colour denoting the class. The coordinates and classes can be extracted by subtracting the dotted and the pair non-dotted training image and running a blob detector on the result. However, this pre-processing step is a rather big source of errors in the training data used for our model. Population counts from the CSV and the extracted dotted images are shown in Table 2.

The given training images are large (sizes 3744x5616, 4992x3328 and 5616x3744). We slice them into 224×224 input images for training and testing. We split the given training set into a training and dev set (80%-20%). The resulting dataset has 21,683 images for training and 5243 for dev.

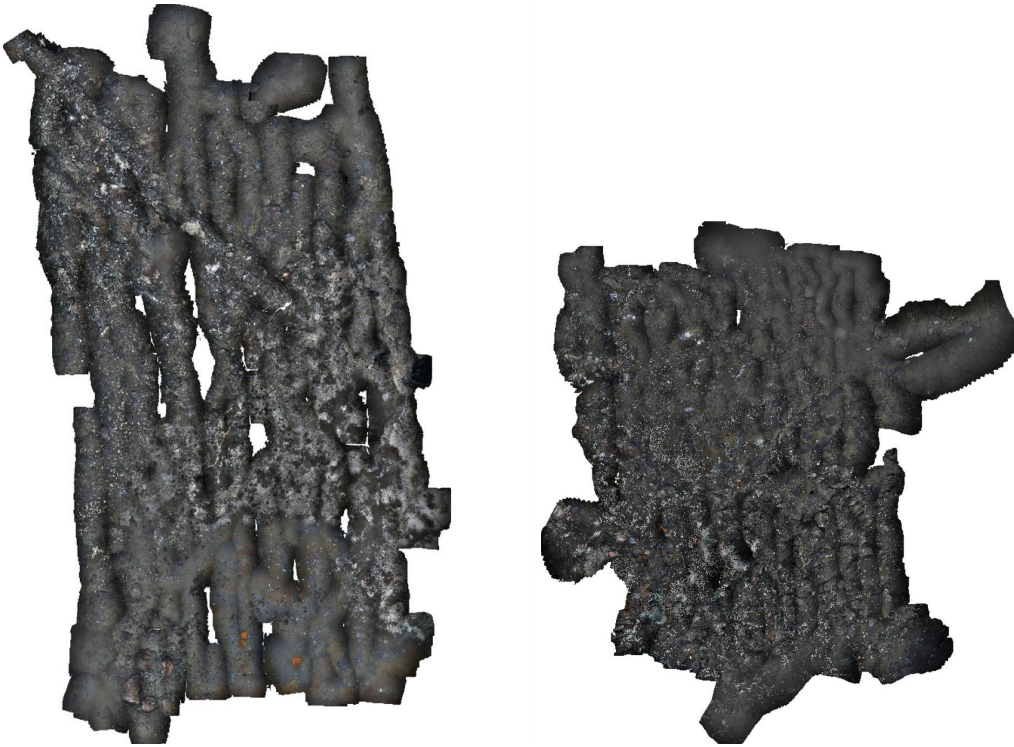
The competition goal, and evaluation criteria, is the final population counts per image rather than predicting where each individual is in the image.

5 Training and evaluation

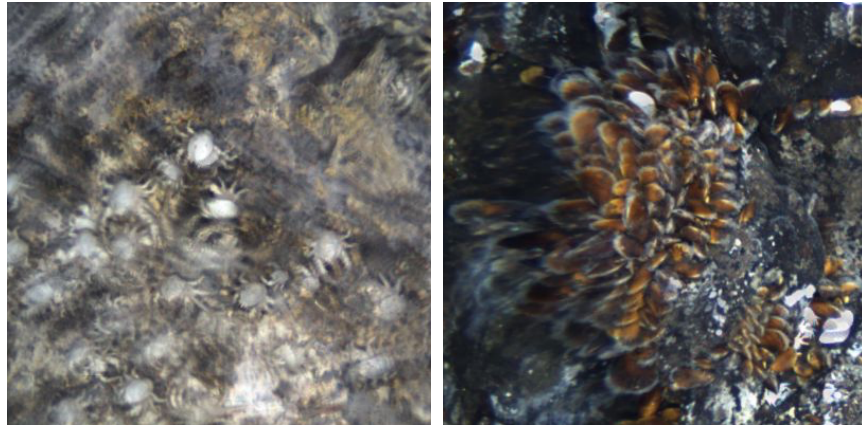
A set of model configurations and hyper-parameters were chosen to train and evaluate our network with. The CNN used to create a feature map is arguably the most important configuration choice.



(a) Examples of original images from the crabs dataset.



(b) The two mosaics of the crabs dataset. Left: C0014G_2m_2014, right: NBC_2m_2014.



(c) Two close-ups in the mosaics highlighting the effects of image quality loss, likely due to overlapping and image processing for creating the mosaic.

Figure 3: Representation of the crabs dataset with example original images, the map mosaics from which the training data is sliced and highlights of image quality loss in the mosaics.

Table 3: Model evaluation on the crabs dataset with all classes used. 7x7 and 4x4 denote the grid sizes used and slicing states the method of slicing the mosaics into training images. For slicing around objects, the training set is based on the NBC mosaic, the dev set on C0014G and the test set is sequentially sliced. Class values show AP %, mAP in %.

	Sliced sequentially						Sliced around objects					
	4x4			7x7			4x4			7x7		
	Train	Dev	Test	Train	Dev	Test	Train	Dev	Test	Train	Dev	Test
Bathymodiolus japonicus	61.12	36.81	38.50	12.41	10.02	10.38	71.00	41.63	22.46	46.65	9.27	9.26
Thermosipho desbruyesi	9.17	9.29	9.19	46.74	28.91	32.53	26.08	9.11	9.12	55.51	25.87	18.08
Bathymodiolus platifrons	60.81	40.81	33.27	52.34	28.65	31.01	75.59	36.14	20.59	61.33	30.38	17.89
Paralomis	12.49	10.02	9.59	11.74	9.48	9.54	14.89	9.30	9.72	20.72	9.15	9.24
Alvinocaridid	11.98	10.30	11.04	50.82	30.34	23.37	46.43	9.81	9.71	60.18	28.05	16.38
Shinkaia crosnieri	56.61	39.71	43.27	9.12	9.10	9.11	69.49	32.71	22.86	44.01	9.10	9.10
mAP	35.36	24.49	24.14	30.53	19.42	19.32	50.58	23.12	15.74	48.07	18.64	13.33

Table 4: Model evaluation on the **crabs-top3** dataset (only top 3 classes used). 7x7 and 4x4 denote the grid sizes used and slicing states the method of slicing the mosaics into training images. For slicing around objects, the training set is based on the NBC mosaic, the dev set on C0014G and the test set is sequentially sliced. Class values show AP %, mAP in %.

	Sliced sequentially						Sliced around objects					
	4x4			7x7			4x4			7x7		
	Train	Dev	Test	Train	Dev	Test	Train	Dev	Test	Train	Dev	Test
Bathymodiolus japonicus	64.02	36.16	38.49	51.04	27.35	29.26	71.55	41.45	23.72	61.61	30.15	19.00
Bathymodiolus platifrons	63.65	38.23	32.94	47.78	29.58	24.22	75.61	36.25	21.01	60.14	28.47	17.89
Shinkaia crosnieri	59.66	35.71	40.61	41.55	25.66	28.63	68.97	32.60	24.06	55.29	24.15	17.26
mAP	62.44	36.70	37.35	46.79	27.53	27.37	72.04	36.77	22.93	59.01	27.59	18.05

We use the Inception-V1 (GoogLeNet) from Szegedy et al. (2015) up to the *Mixed_5c* layer, pre-trained on ImageNet by Google². The weights are not frozen during training.

The input image size is fixed at 224x224. A configurable parameter is the grid size G . The CNN gives $G = 7$ at the *Mixed_5c* layer. For $G = 4$ we add an extra 4x4 stride 1 max pool layer.

The RNN has two parameters, the number of outputs per grid cell, k , and the number of LSTM layers used. We have 2 LSTM layers and $k = 8$ for all experiments.

5.1 Evaluation on crabs dataset

The crabs dataset is prepared according to Section 4.1. The model was trained on the **crabs** dataset (all 6 classes) for 15 epochs using standard data augmentation methods (random rotations, shears, zooms and shifts) to prevent overfitting. We obtain a mean average precision (mAP) of 24.14% for a 4x4 grid and 19.32% for a 7x7 grid on test, however there is a large difference between the top 3 and bottom 3 classes as seen in Table 3 (Sliced sequentially). This is due to the dataset being heavily unbalanced.

A similar training scenario for the **crabs-top3** dataset yields 37.5% mAP using a 4x4 grid and 27.37% mAP for the 7x7 grid. Results are shown in Table 4 (Sliced sequentially).

As stated in Section 4.1, sequentially slicing the two mosaics results in a relatively tiny dataset for deep models. We therefore slice the mosaics to produce one image for each object by cutting out around the object coordinates. This creates many overlapping images which can be seen as a data augmentation technique. We pick one mosaic for training and one for testing. The dev set is sliced around objects and the test set is sequentially sliced. We trained the models for 15 epochs. We ran this experiment four times, using each mosaic as training in turn and using all or only the top 3 classes. All experiments overfit the training set and perform the poorest on the test set. Results are in Tables 3 and 4 (Sliced around object).

Example predictions are shown in Figure 4, where we can observe the model does large localisation errors but at the same time it predicts good population densities. The locations of predicted crabs tend to form a circle centred near the middle of the grid cells.

²Weights available at <https://github.com/tensorflow/models/tree/master/slim>

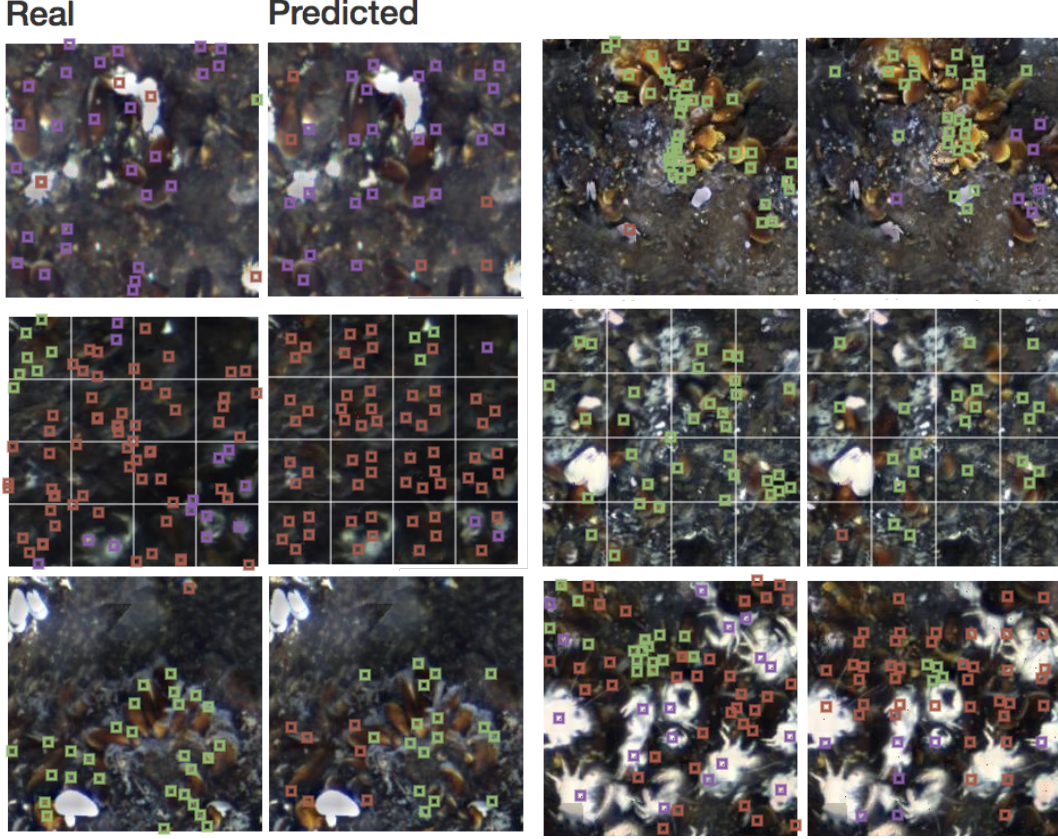


Figure 4: Example predictions on the crabs dataset. The grid is rendered in the middle row for reference. Classes (species) are colour coded. For each image pair, ground truth on left and prediction on right. Confidence threshold 0.5.

5.2 Evaluation on VOC12 dataset

Two models were trained on the VOC dataset, one using a 4x4 grid and one using a 7x7 grid. The resulting mAPs on the dev test are 29.93% and 27.34%, respectively, which are below the state of the art but the model parameters are not fine-tuned for this dataset. We focus mainly on small objects that fit into a grid cell. The training was done with no data augmentation. Table 5 shows per-class average precision (AP) scores and mAP results on train and dev sets.

Large objects that span across many grid cells are predicted more than once, but only considered correct in the cell containing the centre of the ground truth label. This raises the level of false positives at test time and can negatively influence training. For instance, if an object is in the middle between two grid cells, both are equally qualified to make that prediction, but only one will contain the object and during training this situation will be regarded as an error in the other grid cell.

Example predictions are shown in Figure 5

5.3 Evaluation on Steller Sea Lions Dataset

The aim of the NOAA Fisheries Kaggle competition is to predict population counts, not to detect where objects are. The evaluation metric for the competition is mean column-wise root mean squared error (RMSE). For N images and K classes, it is:

$$\frac{1}{K} \sum_i^K \sqrt{\frac{1}{N} \sum_j^N (y_{ij} - \hat{y}_{ij})^2}, \quad (3)$$

where the labels y and predictions \hat{y} are population counts.

Table 5: Evaluation results on the VOC12 detection dataset. Class results are Average Precision (AP). 4x4 and 7x7 denote the grid size of our model configuration. Input images resized to 224x224 pixels. No data augmentation was used and no fine-tuning of the model. Values in %.

	Train 7x7	Train 4x4	Dev 7x7	Dev 4x4
aeroplane	51.66	52.74	36.69	34.29
bicycle	55.19	52.00	22.46	23.37
bird	42.37	52.01	29.04	33.65
boat	45.87	50.67	24.00	27.47
bottle	51.56	46.62	14.79	14.38
bus	69.35	56.27	38.57	35.07
car	52.61	56.92	27.99	32.24
cat	47.69	61.27	31.56	38.95
chair	39.57	52.36	18.57	22.95
cow	57.38	56.83	25.57	31.30
diningtable	54.00	69.85	20.41	24.91
dog	51.58	62.07	31.08	35.35
horse	49.49	61.69	23.50	32.43
motorbike	55.91	58.58	29.69	28.17
person	54.09	65.14	40.60	47.76
pottedplant	40.74	49.22	18.11	21.33
sheep	55.27	60.86	35.92	36.32
sofa	52.88	65.97	16.83	20.28
train	47.68	47.79	30.18	32.39
tvmonitor	51.37	53.66	31.16	25.95
mAP	51.31	56.63	27.34	29.93

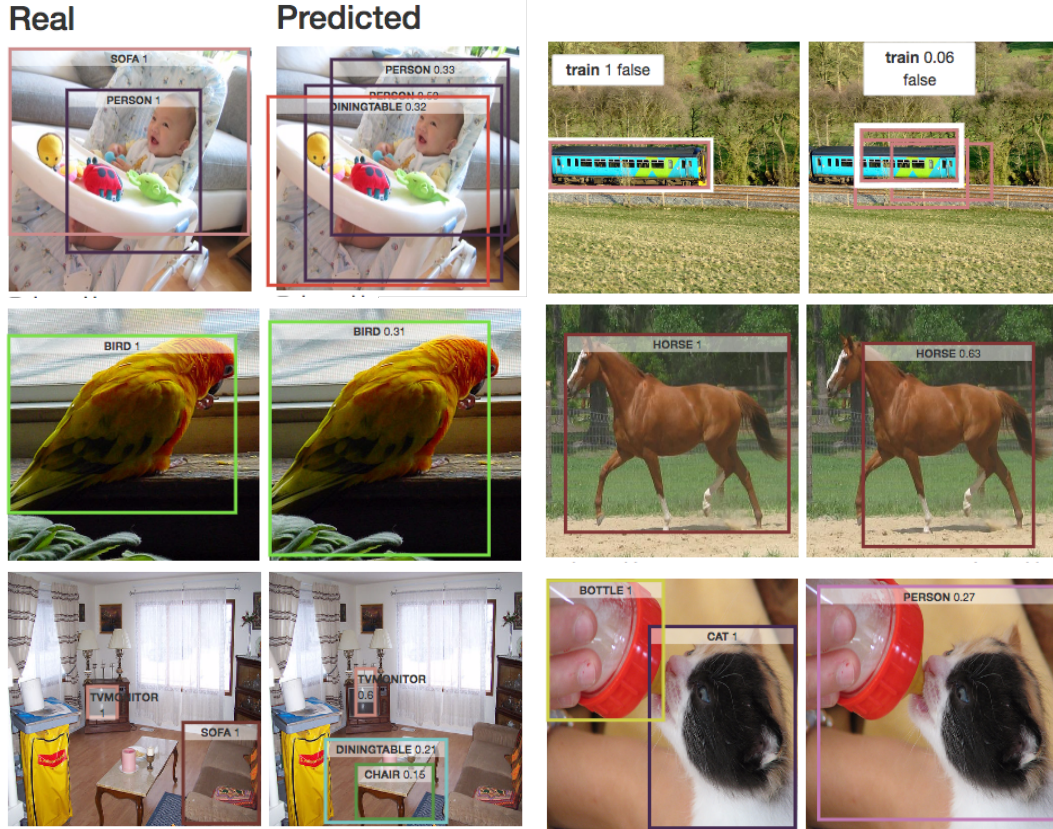


Figure 5: Example predictions on the VOC12 dataset. For each image pair, ground truth on left and prediction on right. Confidence score shown next to object class name.

Table 6: Evaluation results on the Steller Sea Lions dataset. Class results are Average Precision (AP) %. 4x4 and 7x7 denote the grid size of our model configuration. Dataset images sequentially sliced in 224x224 input images. mAP in %. RMSE is Mean Column-Wise RMSE at 0.5 confidence threshold.

	7x7 train	7x7 dev	4x4 train	4x4 dev
adult females	35.68	33.00	45.03	41.92
adult males	49.24	36.77	57.81	45.86
juveniles	39.91	31.87	47.52	38.86
pups	36.38	32.36	43.27	37.98
subadult males	36.01	23.01	48.67	27.04
mAP	39.44	31.40	48.46	38.33
RMSE	1.69	1.68	1.49	1.52

We trained two models, grid 7x7 and grid 4x4. On the dev set we achieve 31.40% and 38.33%, respectively. Training was done for 30 epochs. Mean Column-Wise RMSE at 0.5 confidence threshold for 7x7 and 4x4 are 1.68 and 1.52, respectively. Note this is on the sliced dev set, not on the large images from the original dataset. The values will likely be higher on the larger images. Results illustrated in Table 6. At the time of writing, the top position in the competition leaderboard has 11.33729 RMSE on the official test set.

6 Implementation

The model was developed with TensorFlow (Abadi et al., 2015). I used parts of TensorBox³ (TensorFlow implementation of (Stewart et al., 2016)) as a reference point. My implementation is an object detection network as opposed to only object localisation like TensorBox.

I implemented image and label readers for VOC, sea lions and crabs datasets along with tools used for slicing images and labels. I implemented an evaluation, prediction and visualisation tool. The predictions are stored in an sqlite databases and can be later used for visualisation and further analysis.

The visualisation tool allows viewing all trained models in a directory tree along with relevant evaluation results on test, dev and training sets. The visualisation tool is a python (with flask) web server and web page that shows evaluation metrics, class counts, images and predictions on the images and precision-recall plots. A screenshot is shown in Figure 6.

References

- Martín Abadi, Ashish Agarwal, Paul Barham, Eugene Brevdo, Zhifeng Chen, Craig Citro, Greg S. Corrado, Andy Davis, Jeffrey Dean, Matthieu Devin, Sanjay Ghemawat, Ian Goodfellow, Andrew Harp, Geoffrey Irving, Michael Isard, Yangqing Jia, Rafal Jozefowicz, Lukasz Kaiser, Manjunath Kudlur, Josh Levenberg, Dan Mané, Rajat Monga, Sherry Moore, Derek Murray, Chris Olah, Mike Schuster, Jonathon Shlens, Benoit Steiner, Ilya Sutskever, Kunal Talwar, Paul Tucker, Vincent Vanhoucke, Vijay Vasudevan, Fernanda Viégas, Oriol Vinyals, Pete Warden, Martin Wattenberg, Martin Wicke, Yuan Yu, and Xiaoqiang Zheng. TensorFlow: Large-scale machine learning on heterogeneous systems, 2015. URL <http://tensorflow.org/>. Software available from tensorflow.org.
- M. Everingham, S. M. A. Eslami, L. Van Gool, C. K. I. Williams, J. Winn, and A. Zisserman. The pascal visual object classes challenge: A retrospective. *International Journal of Computer Vision*, 111(1):98–136, January 2015.
- Lowell W Fritz, Kathryn M Sweeney, Rodney G Towell, and Thomas Scott Gelatt. *Aerial and Ship-based Surveys of Steller Sea Lions (Eumetopias Jubatus) Conducted in Alaska in June-July 2013 Through 2015, and an Update on the Status and Trend of the Western Distinct Population Segment in Alaska*. 2016.
- Tsung-Yi Lin, Michael Maire, Serge Belongie, James Hays, Pietro Perona, Deva Ramanan, Piotr Dollár, and C Lawrence Zitnick. Microsoft coco: Common objects in context. In *European Conference on Computer Vision*, pp. 740–755. Springer, 2014.

³<https://github.com/TensorBox/TensorBox>

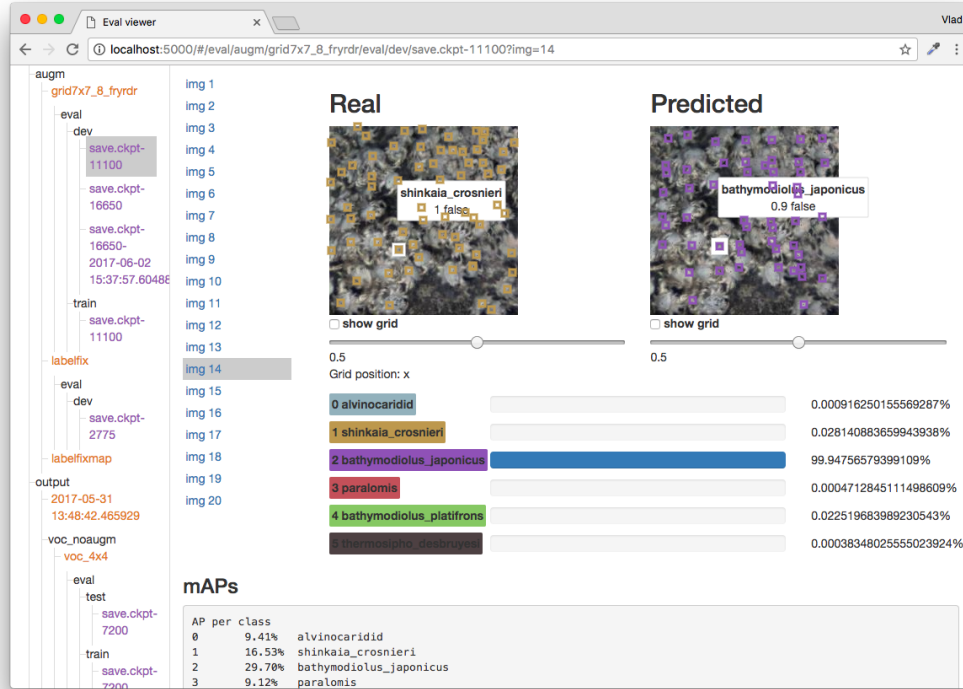


Figure 6: Screenshot of the visualisation tool built to aid the development of this model. The predictions seen in the page are all misclassified. Highlighting shows matching pair of ground truth and prediction.

NOAA Fisheries. Noaa fisheries steller sea lion population count, 2017. URL <https://www.kaggle.com/c/noaa-fisheries-steller-sea-lion-population-count>.

Joseph Redmon, Santosh Divvala, Ross Girshick, and Ali Farhadi. You only look once: Unified, real-time object detection. In *Proceedings of the IEEE Conference on Computer Vision and Pattern Recognition*, pp. 779–788, 2016.

Russell Stewart, Mykhaylo Andriluka, and Andrew Y Ng. End-to-end people detection in crowded scenes. In *Proceedings of the IEEE Conference on Computer Vision and Pattern Recognition*, pp. 2325–2333, 2016.

Christian Szegedy, Wei Liu, Yangqing Jia, Pierre Sermanet, Scott Reed, Dragomir Anguelov, Dumitru Erhan, Vincent Vanhoucke, and Andrew Rabinovich. Going deeper with convolutions. In *Proceedings of the IEEE Conference on Computer Vision and Pattern Recognition*, pp. 1–9, 2015.

Blair Thornton, Adrian Bodenmann, Oscar Pizarro, Stefan B Williams, Ariell Friedman, Ryota Nakajima, Ken Takai, Kaori Motoki, Tomo-o Watsuji, Hisako Hirayama, et al. Biometric assessment of deep-sea vent megabenthic communities using multi-resolution 3d image reconstructions. *Deep Sea Research Part I: Oceanographic Research Papers*, 116:200–219, 2016.